# Inertial Aiding for Moving GPS Receiver Carrier Phase Estimation Through Wideband Interference


1st Wengxiang Zhao
*Mechanical, Material, and Aerospace Engineering Department*
*Illinois Institute of Technolgy*
Chicago, USA
wzhao42@hawk.iit.edu

2nd Samer Khanafseh
*Mechanical, Material, and Aerospace Engineering Department*
*Illinois Institute of Technolgy*
Chicago, USA
khansam1@hawk.iit.edu

3rd Boris Pervan
*Mechanical, Material, and Aerospace Engineering Department*
*Illinois Institute of Technolgy*
Chicago, USA
pervan@iit.edu



***Abstract*—In this paper, we extend prior research on Interacting Multiple Model (IMM) Kalman filtering for GPS carrier phase estimation through wideband interference from static to moving receivers. In preparation, we develop a vibration dynamic model for the clock and a carrier-to-noise ratio estimator applicable in interference condition. We couple a Inertial Measurement Unit (IMU) with the GPS receiver to provide inertial aiding for user dynamics.**



***Keywords—GPS carrier phase estimation, interference mitigation, IMU inertial aiding***


## I. INTRODUCTION

Along with the growing demand of GPS services, intentional and unintentional jamming and spoofing are happening more frequently than in the past [1]. The goal of this research is to develop a robust GPS receiver to estimate the carrier phase and preserve the continuity during wideband radio frequency interference (RFI) events.

In a traditional Phase Lock Loop (PLL) approach, tracking GPS signals through strong RFI requires coherent integration times ($T_{coh}$) longer than the length of a GPS Navigation Data (ND) bit (20 ms). However, using larger values of $T_{coh}$ means integrating I (in-phase) and Q (quadrature) samples across ND bit transitions. Potential PLL-based solutions to extend averaging time, such as non-coherent memory discriminators [2] or real-time bit estimation techniques [3], introduce biases in the discriminator output, which cause errors in reconstructed carrier Doppler and ultimately lead to cycle slips.

Kalman Filters (KF) have been used to estimate carrier phase through ionospheric scintillation in [4][5] with $T_{coh}$ < 20 ms and to track weak GPS signals with $T_{coh}$ > 20 ms in [6] using a novel Bayesian approach for ND bit estimation. The Interacting multiple model (IMM) algorithm generalizes the concept using multiple KFs with different hypothesized data bits and noise models. It then combines the estimation outputs from the different KFs at each $T_{coh}$ time step using the posterior probabilities of each hypothesized mode to avoid $2n$ exponential growth of the number of models as $n$ bits of ND are processed.

In prior work [7], we derived a phase noise dynamic model for a rubidium receiver clock to effectively enable IMM/KF phase averaging across ND bit boundaries. We then implemented and experimentally validated the IMM/KF carrier phase estimation performance for static receivers under deteriorated carrier-to-noise ratio conditions down to 15 dB/Hz. In [8] and [9], we demonstrated the superior performance of the IMM/KF over the PLL as measured by carrier phase estimation error variances, and we introduced partial prediction of ND bits to further improve phase estimation results. In [10], we demonstrated that essentially the same performance was achievable without an atomic clock and that commercial TCXO and OCXO oscillators were also sufficient.

In this paper, we add a tightly coupled IMU to compensate for the Doppler introduced by a moving receiver. Because the clock is no longer on a stable (static) platform, we also derive a vibration clock phase noise power spectral density (PSD) model using the method in [11]. This vibration clock phase noise PSD can also be used in future aircraft applications. Based on current methods for carrier to noise ratio ($C/N_0$) estimation [12][13][14], we develop an unbiased $C/N_0$ and signal amplitude estimator that works at $C/N_0$ as low as -10 dB/Hz and does not assume phase-lock. We validate analysis and simulation results with automobile road tests using received signals from the GPS satellites summed with broadband RFI generated by an RF signal simulator in the car.

In Section II, the IMM algorithm is explained and the component Kalman filters are set up. Section III derives a debiased moment matching $C/N_0$ estimator. Section IV introduces the Doppler shift calculation. Section V presents the result from in lab static test. Section VI shows the result from road test.

## II. IMM KALMAN FILTER

The Kalman filter is an optimal state estimator for systems with additive white Gaussian noise (AWGN). In this research we are interested in wideband RFI, which is AWGN. Reconsidering the tracking of carrier phase, we recognize that it is essentially an estimation problem. A PLL or KF takes the information from $I$ and $Q$ samples and by leveraging knowledge of the dynamic limitations of the receiver platform, produces estimates for current carrier phase and frequency. We leave the sampling elements of traditional PLL structure unchanged but replace its discriminator and loop filter with a KF.

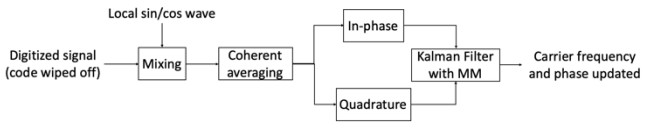


Fig. 1. KF in carrier phase estimation loop

### A. *Clock Vibration* Dynamic *Model*

In our prior work [7], we derived the clock dynamic model as

$$\begin{bmatrix} A \\ \phi_{clk} \\ f_{clk} \end{bmatrix}_{k+1} = \begin{bmatrix} 1 & 0 & 0 \\ 0 & 1 & T_{coh} \\ 0 & 0 & 1 \end{bmatrix} \begin{bmatrix} A \\ \phi_{clk} \\ f_{clk} \end{bmatrix}_{k} + \omega_k \quad (1)$$

where

$$W = \begin{bmatrix} \delta^2 & 0 & 0 \\ 0 & S_f T_{coh} + \frac{S_g {T_{coh}}^3}{3} & \frac{S_g {T_{coh}}^2}{2} \\ 0 & \frac{S_g {T_{coh}}^2}{2} & \frac{S_f}{T_{coh}} + \frac{4 S_g T_{coh}}{3} \end{bmatrix} \quad (2)$$

and $\delta^2 \approx 0$,

$$S_g = 2\pi^2 h_{-2} \quad (3)$$

$$S_f = \frac{h_0}{2} \quad (4)$$

$$h_{-2} = 2.4819 \times 10^{-12} \quad (5)$$

$$h_{-2} = 1.241 \times 10^{-6}. \quad (6)$$

The phase noise power spectrum density (PSD) is:

$$S(f) = \frac{{f_0}^2}{f^2}(h_{-2} f^{-4} + h_0 f^{-2}) . \quad (7)$$

In vibration case the phase noise PSD will increase by [10]:

$$S_{\phi,vib}(f) = (k_g N f_0)^2 \frac{S(f)}{f^2} \quad (8)$$

where $k_g$ is the oscillator's acceleration sensitivity in parts/g and $N$ is the acceleration in g. Here we consider the worst free-falling case, $2 \times 10^{-10}$ for $k_g N$ in our case from the specification value. Later on, we can modify the $N$ from the IMU output z axis acceleration.

### B. Measurement *Model*

The IMM Kalman filter takes I and Q samples as measurements:

$$I_k = A_k d_k \cos(\phi_{clk,k}) + v_{i,k} \quad (9)$$

$$Q_k = A_k d_k \sin(\phi_{clk,k}) + v_{q,k} , \quad (10)$$

where $d_k$ is the navigation data bit at time epoch $k$, $A_k$ is the signal amplitude, $v_{i,k}$ and $v_{q,k}$ are i.i.d. $\sim N(0, V)$ with $V = I\sigma_v^2$ , and $\sigma_v^2$ is defined by the carrier to noise ratio as

$$C/N_{0,k} = 10^{\frac{C/N_{0,k}[dB/Hz]}{10}} \quad (11)$$

$$\sigma_{v,k}^2 = \frac{1}{2\, T_{coh}\, C/N_{0,k}} . \quad (12)$$

### C. *IMM Filter*

The IMM algorithm is a method for combining state hypotheses from multiple filter models to get a better state estimate of targets with changing dynamics. It works for those systems that have multiple model whether in dynamics or measurements. In our case, the uncertain in navigation data bits can be covered by two modes in IMM filter. Figure 2 is the illustration of the logic of our IMM filter.

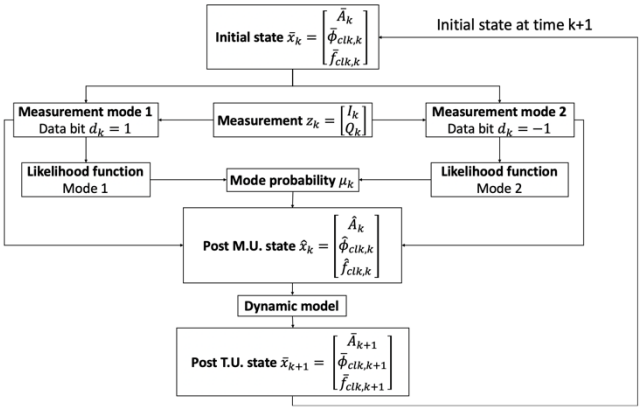


Fig. 2. IMM filter

## III. Carrier to Noise Ratio Estimator

The measurement model noise level is highly dependent on the carrier-to-noise ratio, which can vary widely because we are specifically interested in wideband interference scenarios. Assuming an incorrect $C/N_0$ can lead to failure in carrier phase estimation. For example, assuming there is a wideband interference event causing the $C/N_0$ to drop from 45 dB/Hz to 20 dB/Hz, if IMM Kalman filter does not adapt it will still process the measurement update with the noise level at 45 dB/Hz. Thus, the increased measurement noise will feed the filter which is still trusting the measurements much more than it should. The filter will not adequately reject noise unless it is updated with the current $C/N_0$ information.

A real-time carrier to noise ratio estimator is needed to assist the IMM filter to adapt to the interference event. There are some methods for $C/N_0$ estimation such as the traditional power ratio method [12], estimation of distribution parameters (Koay's method) [13], maximum likelihood methods [14] and moment matching methods [15]. However, all these methods are designed to work at 'normal' signal strength levels and will produce biased estimation results for low $C/N_0$ . For example, power ratio method, which is the most commonly used, only generates reliable estimates when $C/N_0$ is above 25 dB/Hz.

For a typical commercial GPS receiver, there is little point in estimating $C/N_0$ lower than 35 dB/Hz since the receiver PLLs can't maintain carrier lock in that range anyway. But our prior work shows that the IMM Kalman filter can coast through wideband interference with $C/N_0$ as low as 15 dB/Hz. In our prior experimental tests, we collected data from an RF simulator so that we had control of everything, including knowledge of $C/N_0$. However, in real applications we will need to rely on our own $C/N_0$ estimator.

### A. *Debiased Moment Matching* $C/N_0$ *Estimator*

Figure 3 shows simulation results from $C/N_0$ estimation using five different methods. We generate $I$ and $Q$ data samples from 15 dB/Hz to 45 dB/Hz as inputs into these five

estimators. In Figure 3, we plot the output $C/N_0$ estimation result vs. the actual input $C/N_0$.

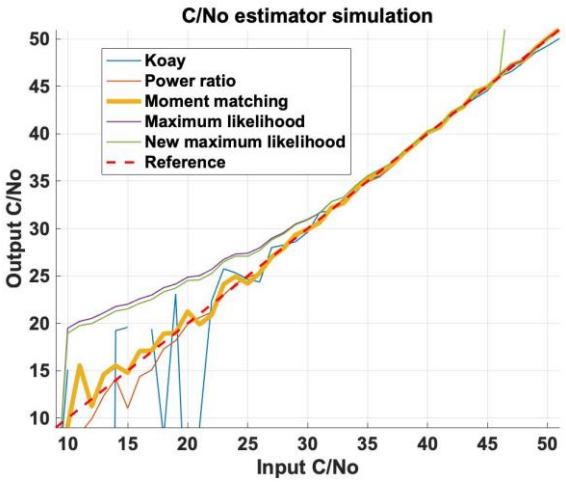


Fig. 3. $C/N_0$ estimation simulation results

The red dashed line is the reference line —a diagonal line from (10, 10) to (50, 50). The closer an estimator lies to the reference line, the better estimation performance it has. All five colored lines are nearly on top of the reference line while the input $C/N_0$ is above 35 dB/Hz. However, when the $C/N_0$ starts dropping below that, all the colored lines deviate from the reference line, with the most significant deviations seen for Koay's method, the maximum likelihood method, and the new maximum likelihood method.

We choose the moment matching method for the further investigation because the estimation bias at the low $C/N_0$ range is more predictable than the power ratio method. We then empirically derive a de-biasing equation for $C/N_0$ estimation result lower than 10 dB/Hz as:

$$C/N_0 = \frac{20}{(\log_{10}(10\times T)\times 2.5+10)\times(C/N_{0,biased}-10)} + 10 \quad (13)$$

where $T$ is the averaging time for $I$ and $Q$ samples in the $C/N_0$ estimator. Figures 4 and 5 show the $C/N_0$ and signal amplitude estimation results using the de-biased moment matching estimator.

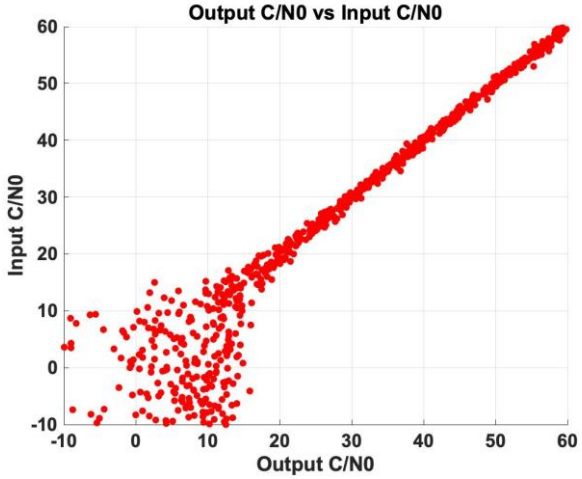


Fig. 4. $C/N_0$ estimation using debiased moment matching

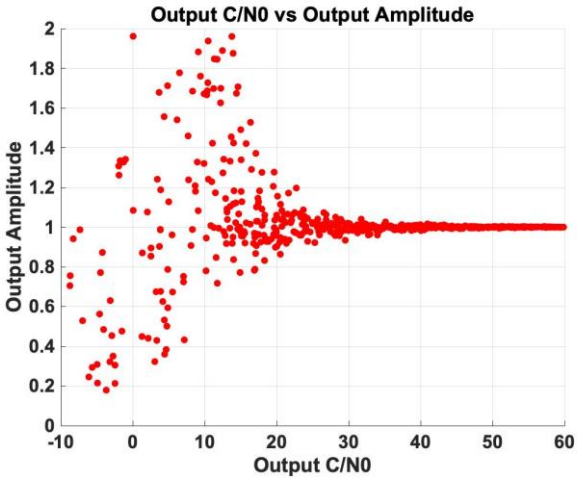


Fig. 5. Amplitude estimation using debiased moment matching

Figure 4 shows reasonably accurate $C/N_0$ estimation results down to -10 dB/Hz. Figure 5 shows the signal amplitude estimation result for an input reference amplitude of 1. Unlike $C/N_0$ estimation, the amplitude estimation has larger errors in the low $C/N_0$ range.

### *B. Real Data Test*

We test our debiased moment matching estimator with a real data set generated by an RF simulator. We set the $C/N_0$ to 51 dB/Hz before interference and 15 dB/Hz during the interference. Figure 6 is the result we use 20 ms averaging time for one $I$ and $Q$ sample and collect 50 such samples to produce one $C/N_0$ estimate. Thus, $C/N_0$ is being updated at 1 second time intervals.

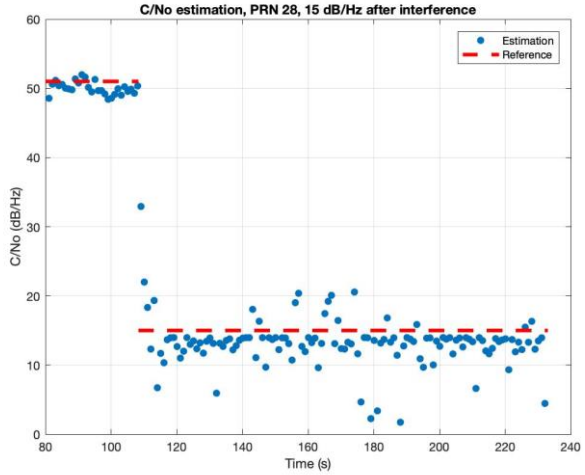


Fig. 6. $C/N_0$ estimation result with 1-second update interval

The red dashed line is the input reference and blue dots are the $C/N_0$ estimation output. The $C/N_0$ estimation output is centered around reference line for low $C/N_0$ as 15 dB/Hz. We then vary the update (i.e., averaging) interval for the estimator, setting it to 0.2 seconds and 5 seconds and test with the same data set used in the 1 second results. The results are shown in Figures 7 and 8.

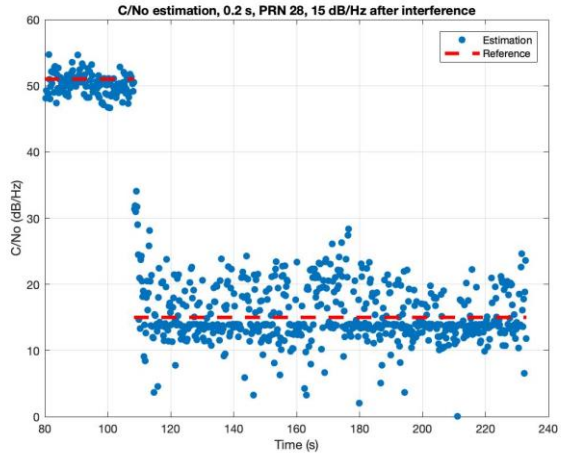


Fig. 7. $C/N_0$ estimation result with 0.2-second update interval

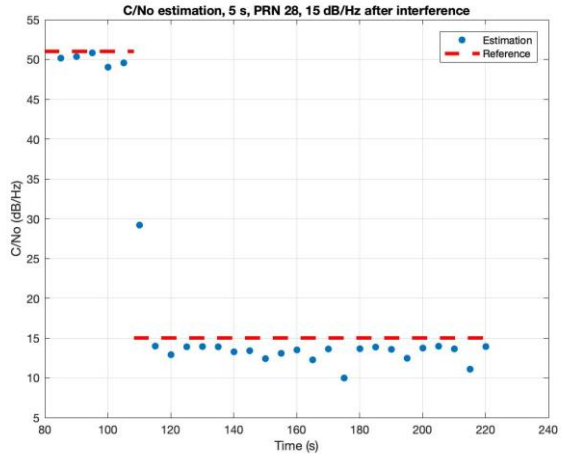


Fig. 8. $C/N_0$ estimation result with 5-second update interval

With the shorter update interval, we have more outputs in same time window, but they are not as accurate as 1 second result. For the longer update interval, the results are more accurate but react slower to any $C/N_0$ change. In Figure 8, there is a single data point around 30 dB/Hz, that is the output from half data before and half data during interference. The IMM filter will use this 'wrong' value for the next 5 seconds which may lead to inaccurate carrier phase measurement result. Taking these two competing factors into account, we decide to use 1 second as the update rate of our $C/N_0$ estimator.

We are also interested in the lowest $C/N_0$ at which our estimator can work reliably. So, we generate another data set using the RF simulator, starting with 40 dB/Hz and making a staircase attenuation down to 5 dB/Hz. The results in Figure 9 show that our estimator performs well until about 12 dB/Hz, but fails at 5 dB/Hz.

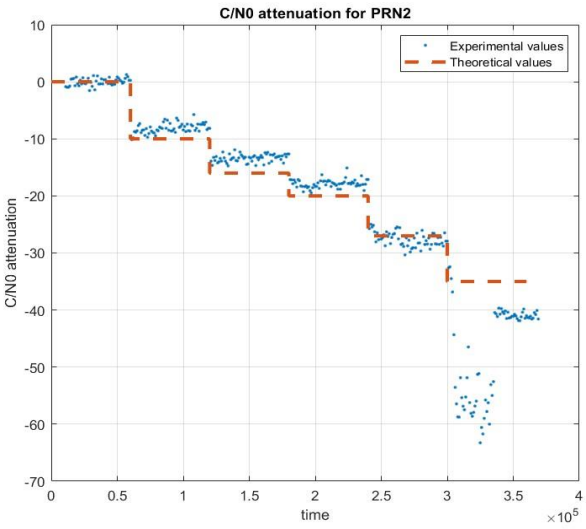


Fig. 9. $C/N_0$ estimation results with staircase attenuation

## IV. Inertial Aiding

An Inertial Measurement Unit (IMU) is a device that can measure and report specific force and angular rate of an object to which it is attached. By providing the GPS receiver with IMU measurements, we can largely remove higher frequency user motion from the carrier phase estimation problem. We use the velocity output from the IMU to calculate the Doppler shift between user and satellite. The position of satellite in ECEF frame as well as the line of sight vector can be directly calculated from the broadcasted ephemerides.

Once we have the relative velocity vector between the user and satellites and the line of sight vector from user to the satellite, the Doppler can be calculated as:

$$f_{Doppler} = (e^T v)\frac{f_{L1}}{c} \tag{14}$$

Examples of the user velocity profile and resulting Doppler profiles for two satellites are shown in Figures 10 and 11, respectively, using a static IMU placed on a lab bench.

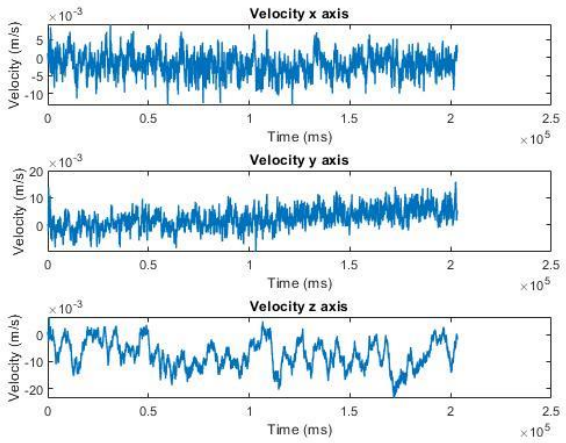


Fig. 10. User velocity output from a static IMU

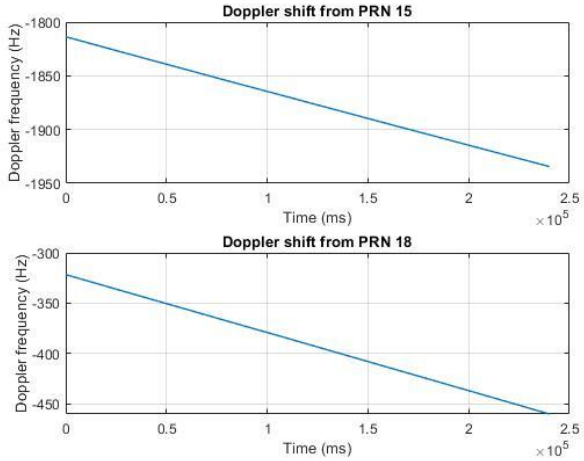


Fig. 11. Doppler profiles for two sattelites

## V. In-Lab Static Test

With a $C/N_0$ estimator that works in low $C/N_0$ range and inertial aiding from the IMU, we are ready to test our IMM KF filter in lab under static conditions. Although the IMU is placed on a bench and kept still throughout the test, the estimator assumes it is moving and uses its outputs for inertial aiding.

### A. Experimental Setup

Figure 12 is an overview of our experimental setup, and Figure 13 shows a breakdown of the constituent elements of the system.

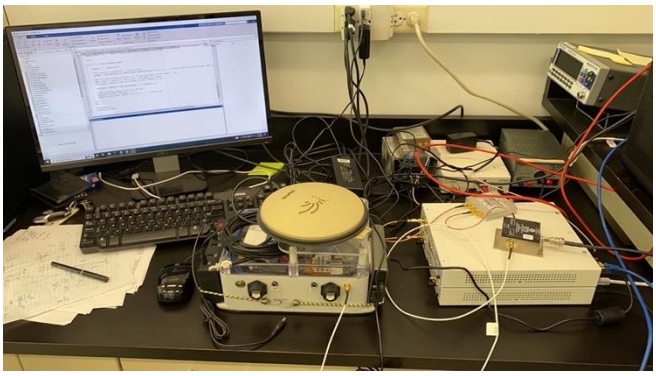

Fig. 12. Overview of the experimental setup

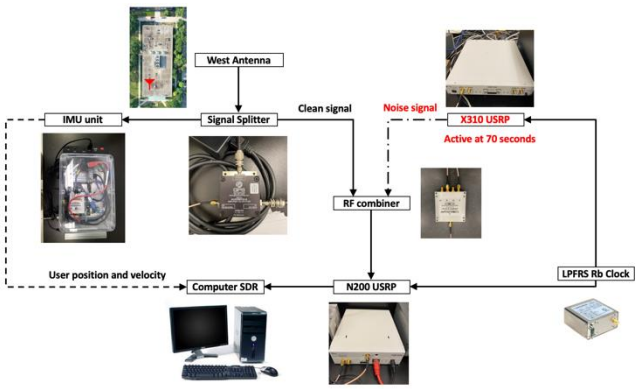


Fig. 13. Flowchart of the experimental setup

We use an antenna mounted on our building rooftop to provide the RF signal input. This RF signal is split into two parts, one feeding an independent tightly coupled GPS/IMU to serve as a truth reference, the other into an RF combiner to sum the clean signal from the rooftop antenna with a wideband noise signal generated by a USRP (X310) to imitate an interference event.

We collect 2 minutes of data. The first half is a clean signal and the second half is a clean signal plus wideband noise. For the first minute, we do not turn on the USRP (X310), so the RF combiner sums the clean signal with nothing from USRP (X310) side. For the next minute, we turn on the USRP (X310) to generate noise RF signal. The output from the RF combiner is then the clean signal plus the noise signal.

The output from RF combiner is collected by another USRP (N200), sampled, and send into a computer for the SDR to process. Two independent LPFRS Rb clocks are used as the time standards for the two USRPs. Also, the output from the IMU is sent to the computer for inertial aiding.

### B. Results

Figure 14 shows the carrier to noise ratio $C/N_0$ estimation result for this scenario.

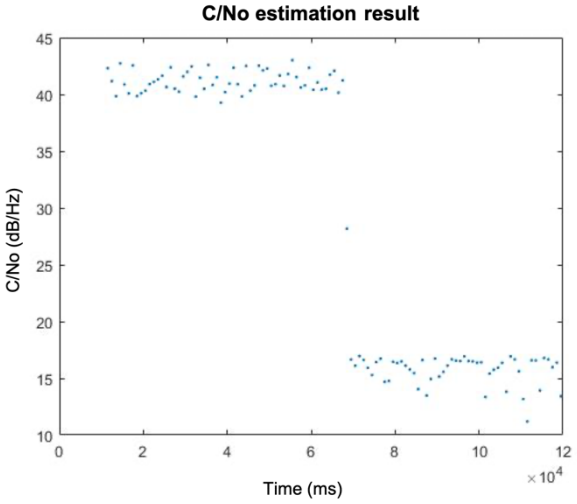


Fig. 14. $C/N_0$ estimation for the in-lab static test

Figure 15 shows the IMM filter carrier frequency estimation error (red). For comparison we also show the output of a typical PLL (blue). The carrier frequency estimation error from the IMM filter maintains a zero mean throughout the test, whereas the PLL output grows without bound after the interference onset (at 60 seconds). Figure 16 and 17 are zoomed-in versions of Figure 15.

The results of the in-lab static test show that our IMM filter is able to provide a good carrier phase and frequency estimation during an interference event.

## VI. Road Test

We then moved our experimental setup from the lab to a car platform.

### A. Experimental Setup

Figure 18 shows that we placed an antenna on top of the car to collect dynamic RF signal data. The car drove at a moderate speed (approximately 1 m/s) along the x-axis direction (northward) within one of our university's parking lots, as shown in Figure 19. We transferred the equipment from Figure 12 to the car trunk, as shown in Figure 20.

We collected 3 minutes of data with an inserted interference event that started at 90 seconds. Figures 21 and 22 show the signal spectrum before and during the interference event, respectively. Before the interference event, there was a clear signal peak centered on the GPS L1 frequency. During the interference event, this peak was buried under a high-power, wideband radio frequency interference signal.

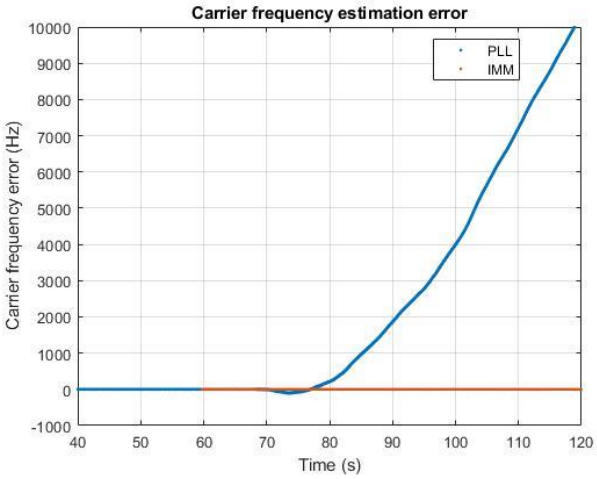


Fig. 15. Carrier frequency estimation error for the in-lab static test

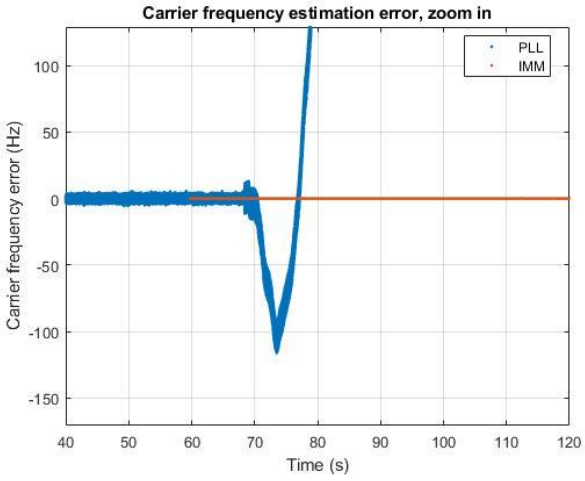


Fig. 16. In-lab static test, zoomed in

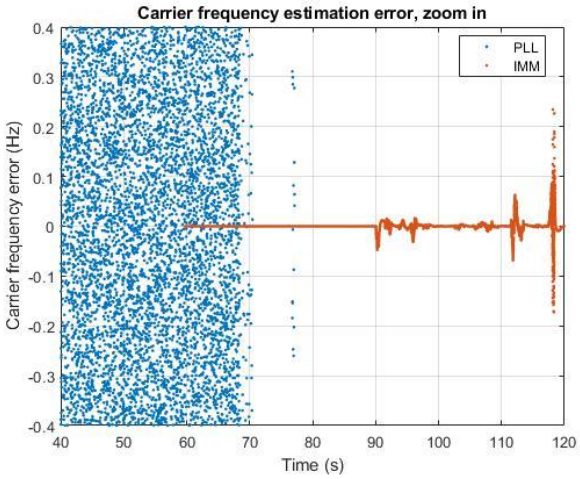


Fig. 17. In-lab static test, zoomed in again

The IMU output of user velocity is shown in Figure 23. We initialized our IMU with a static position and then began driving and collecting data. The velocities on the x and y axes reflect our driving speed, and the velocity on the z-axis is due to vibration.


Fig. 18. Antenna on top of the car


Fig. 19. Moving user trajectory

Fig. 20. Road test setup

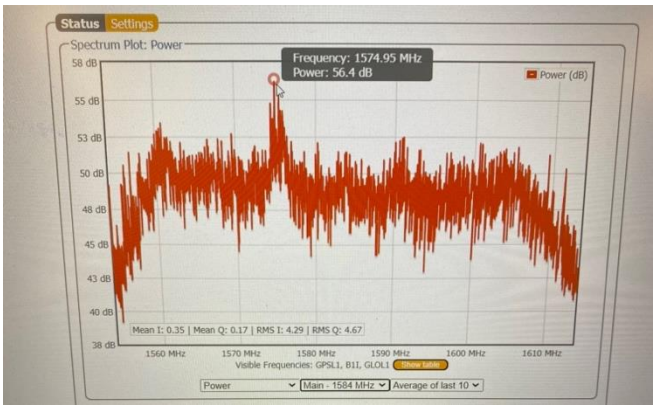


Fig. 21. Spectrum before the interference

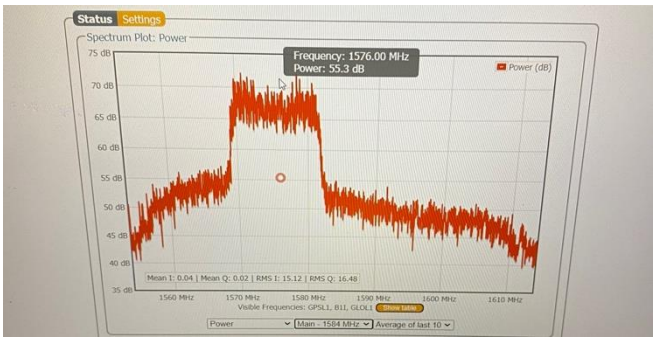


Fig. 22. Spectrum during the interference

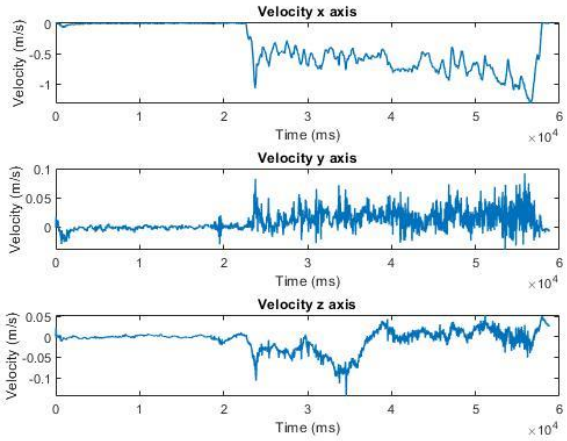


Fig. 23. IMU velocty ouput during the test

Similarly, we applied the IMM Kalman filter to the data and performed inertial aiding to account for user dynamics. We show the results of the carrier frequency estimation error from one PRN.

Figure 24 shows results similar to those we obtained in the lab test: the PLL is not able to track the carrier frequency once the interference event starts. Figure 25 is a zoomed-in version of Figure 24, showing zero-mean frequency estimate error from the IMM filter during jamming.

The standard deviation of the IMM filter estimate error output is slightly larger than in lab test (Figure 17), which may be due to increased clock phase and frequency noise caused by the vibration during driving. Overall, we can claim that our IMM filter is able to maintain GPS receiver continuity during the strong RFI event.

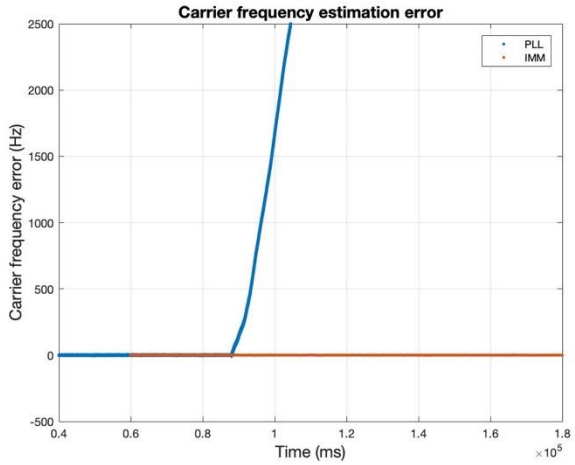


Fig. 24. Road test result

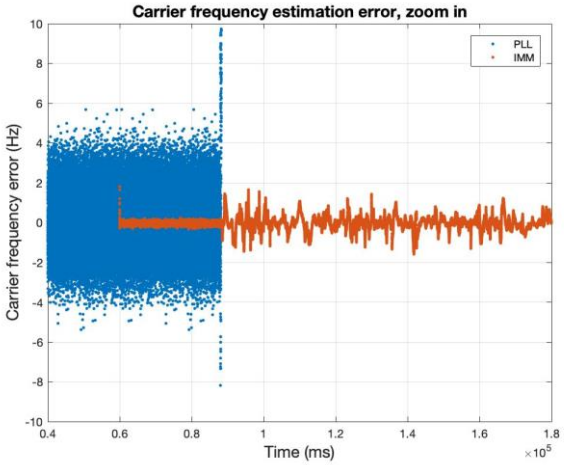


Fig. 25. Road test result, zoomed in

## CONCLUSION

In this research, we developed a debiased carrier-to-noise ratio estimator that solves the historical problem of low-range carrier-to-noise ratio estimation. We tested the estimator with real data at various levels of carrier-to-noise ratio and produced unbiased estimation results. We then integrated the real-time carrier-to-noise ratio into an IMM filter and tested the latter's ability to estimate carrier frequency under strong wideband interference conditions, first with in-lab static data and then using a moving receiver with inertial aiding. The GPS receiver with the IMM filter did not lose lock throughout the wideband RFI event.

## ACKNOWLEDGMENT

We would like to thank our sponsors at the Federal Aviation Administration (FAA) for supporting this research. The views and opinions expressed in this paper are those of the authors and do not necessarily reflect those of any other organization or person.

## REFERENCES

[1] Pullen, Sam, and G. Xingxin Gao. "GNSS jamming in the name of privacy: Potential threat to GPS aviation." Inside GNSS 7.2 (2012): 34-43.

[2] Borio, Daniele, and Gérard Lachapelle. "A non-coherent architecture for GNSS digital tracking loops." annals of telecommunications-annales des télécommunications 64 (2009): 601-614.

[3] Stevanovic, Stefan, and Boris Pervan. "Coasting Through Wideband Interference Events using Robust Carrier Phase Tracking." Proceedings of the 30th International Technical Meeting of the Satellite Division of The Institute of Navigation (ION GNSS+ 2017). 2017.

[4] Vila-Valls, Jordi, Pau Closas, and Carles Fernandez-Prades. "Advanced KF-based methods for GNSS carrier tracking and ionospheric scintillation mitigation." 2015 IEEE Aerospace Conference. IEEE, 2015.

[5] Humphreys, Todd E., Mark L. Psiaki, and Paul M. Kintner. "Modeling the effects of ionospheric scintillation on GPS carrier phase tracking." IEEE Transactions on Aerospace and Electronic Systems 46.4 (2010): 1624-1637.

[6] Psiaki, Mark L., and Hee Jung. "Extended Kalman filter methods for tracking weak GPS signals." Proceedings of the 15th international technical meeting of the satellite division of the Institute of Navigation (ION GPS 2002). 2002.

[7] Zhao, Wengxiang, and Boris Pervan. "IMM Methods for Carrier Phase Tracking and Navigation Data Bits Estimation Through Interference." Proceedings of the 2019 International Technical Meeting of The Institute of Navigation. 2019.

[8] Zhao, Wengxiang, and Boris Pervan. "Experimental Validation of IMM Algorithm for Carrier Phase Tracking Through Interference." Proceedings of the 2020 International Technical Meeting of The Institute of Navigation. 2020.

[9] Zhao, Wengxiang, and Boris Pervan. "Data Bit Assisted Adaptive IMM Filter for Carrier Phase Tracking Through Interference." Proceedings of the 33rd International Technical Meeting of the Satellite Division of The Institute of Navigation (ION GNSS+ 2020). 2020.

[10] Zhao, Wengxiang, Samer Khanafseh, and Boris Pervan. "Clock Dynamics Analysis in IMM Filter for Carrier Phase Estimation Through Interference." Proceedings of the 34th International Technical Meeting of the Satellite Division of The Institute of Navigation (ION GNSS+ 2021). 2021.

[11] Hegarty, Christopher J. "Analytical Derivation of Maximum Tolerable In-Band Interference Levels for Aviation Applications of GNSS." Navigation 44.1 (1997): 25-34.

[12] Enge, Per, and A. J. Van Dierendonck. "Design of the signal and data format for wide area augmentation of the Global Positioning System." Proceedings of Position, Location and Navigation Symposium-PLANS'96. IEEE, 1996.

[13] Koay, Cheng Guan, and Peter J. Basser. "Analytically exact correction scheme for signal extraction from noisy magnitude MR signals." Journal of magnetic resonance 179.2 (2006): 317-322.

[14] Sijbers, Jan, et al. "Maximum-likelihood estimation of Rician distribution parameters." IEEE Transactions on Medical Imaging 17.3 (1998): 357-361.

[15] Gappmair, Wilfried, Markus Flohberger, and Otto Koudelka. "Moment-based estimation of the signal-to-noise ratio for oversampled narrowband signals." 2007 16th IST Mobile and Wireless Communications Summit. IEEE, 2007.